Applied Catalysis B: Environmental 217 (2017) 466–476

Contents lists available at ScienceDirect

Applied Catalysis B: Environmental

journal homepage: www.elsevier.com/locate/apcatb

Photocatalytic abatement of NOx pollutants in the air using commercial functional coating with porous morphology

Radek Zouzelka[a,b], Jiri Rathousky[a,*]

[a] J. Heyrovsky Institute of Physical Chemistry, v.i.i., Academy of Sciences of the Czech Republic, Dolejskova 3, Prague 18223, Czech Republic
[b] University of Chemistry and Technology Prague, Department of Physical Chemistry, Prague 16628, Czech Republic

ARTICLE INFO

Article history:
Received 16 March 2017
Received in revised form 2 June 2017
Accepted 3 June 2017
Available online 6 June 2017

Keywords:
Photocatalysis
TiO_2
NOx
Gaseous pollutants
Air purification

ABSTRACT

Titanium dioxide is the most important photocatalyst used for purifying applications. The purpose of this study was to investigate the photocatalytic activity of the commercial product Protectam FN2, containing Evonik P25 titanium dioxide nanopowder, with regard to NO and NO_2 abatement. Photocatalytic experiments on the photocatalytic coatings on concrete and plaster substrates were carried out in two types of flow reactors, namely one with laminar flow and another with ideally-mixed flow, under "real world conditions" of temperature, relative humidity, irradiation intensity and pollutant concentrations. The results showed that the photocatalytic process significantly reduced the concentration of both nitrogen oxides in the air. The reaction rate, i.e., the decrease in the concentration of NOx achieved in the steady-state for the inlet concentration of NO and NO_2 of 0.1 ppmv, which corresponds to highly polluted urban air, was up to 75 and 50 $\mu mol\ m^{-2}\ h^{-1}$, respectively, at the flow rate of 3000 $cm^3\ min^{-1}$ and relative humidity of 50%. Further, even two years after their application to the surface of concrete walls along a busy thoroughfare, the photocatalytic coating maintained high effectivity.

1. Introduction

Dangerous nitrogen oxides (NOx) are among the most closely studied gaseous pollutants because of their toxicity to human health. The major source of NOx in Europe is road transport, producing around 40% of the total emissions, comprising a mixture of nitric oxide (NO) and nitrogen dioxide (NO_2). Of the NOx emitted from vehicles, around 80% comes from diesel-powered ones. Because traffic emissions are close to the ground, they contribute relatively more to NO_2 ground concentrations, than, for example, high industrial stacks [1]. European directives impose a limit on NO_2 concentration in ambient air of 40 $\mu g\ m^{-3}$ (0.021 ppmv) averaged over 1 year and of 200 $\mu g\ m^{-3}$ (0.106 ppmv) averaged over 1 h (Directive 2008/50/EC, 2008), which must not be exceeded on more than 18 occasions each year. Concentration limits prescribed by other authorities, such as WHO, the U.S. Environmental Protection Agency, the Ministry of Environmental Protection of China and the Australian Department of the Environment and Energy, are similar [2].

The primary product of combustion in motor vehicle engines is NO, which can be further oxidized to NO_2. The rate of secondary oxidation depends on various meteorological parameters, such as intensity of solar radiation, humidity, presence of pollutants in the air, air flow, among other conditions. While oxidation of NO to NO_2 is not instantaneous, all of the NO present in the air oxidizes to NO_2 within a few hours. Thus, the proportion of both oxides varies considerably throughout a given day [3]. Collectively, this implies that it is necessary to substantially reduce NO concentrations because NO_2 is created solely from NO and ultimately all NO is converted to NO_2. Additionally, there is also very small emission of nitrous acid (HONO), whose concentration is of several orders of magnitude lower than that of NOx. Up to now, there are several studies in which HONO emissions from vehicles were determined. For example, Kessler and Platt (1984) made simultaneous HONO, NO and NO_2 measurements in the hot exhaust gas of gasoline and diesel automobile engines. For gasoline engines operated at high load, HONO/NOx ratios $<10^{-4}$ were determined. Under lean operating conditions, the HONO/NOx ratio increased up to 1.5×10^{-3}. For diesel engines, the HONO/NOx ratio of about 10^{-2} was observed [4]. Pitts et al. (1984) reported the direct spectroscopic detection of HONO in the exhaust from eight light-duty motor vehicles (LDMV). During the warm-up periods, HONO/NOx ratios decreased from 1.8×10^{-2} to $<10^{-3}$ [5]. Kirchstetter et al. (1996) were among the first to study HONO emissions in a traffic tunnel. An average HONO/NOx ratio of $(2.9 \pm 0.5) \times 10^{-3}$ was obtained for a vehicle fleet, which comprised of 67% cars, 33% pickups and small vans,

* Corresponding author.
E-mail address: jiri.rathousky@jh-inst.cas.cz (J. Rathousky).

http://dx.doi.org/10.1016/j.apcatb.2017.06.009

and less than 0.2% heavy-duty trucks [6]. Kurtenbach et al. (2001) estimated the emission index by the vehicles passing through the tunnel as 88 ± 18 mg HONO kg^{-1} fuel [7]. As the concentration of HONO in the air in comparison to NOx is very low, it is of primary importance to reduce the concentration of NO and NO_2.

A decrease in NOx concentrations can be achieved by reducing it to N_2 or by oxidizing it to HNO_3 by a suitable method. Heterogeneous photocatalysis, which is particularly efficient, includes three different processes: photo-decomposition, photo-oxidation and photo-selective catalytic reduction [2]. Because of the need to purify large volumes of air outside buildings, photocatalytic oxidation is the most suitable of these three options to reduce NOx concentrations. In that process, NO is gradually oxidized to nitric acid and NO_2, which in turn is eventually neutralized into various nitrates in the presence of alkali metal or alkaline earth metal ions [8]. This process has been described by the following equation

$$NO \overset{h\nu,\ TiO_2}{\rightarrow} (NO_2)_{ads.} + H_2O \rightarrow HNO_3 \ \text{ or } \ NO_3^- . \quad (1)$$

If there are enough water droplets in the air, due to rain or artificial sprays of water, e.g. fountains, disproportionation of NO_2 to nitric acid and NO occurs, according to the equation

$$3NO_2 + H_2O \rightarrow 2HNO_3 + NO. \quad (2)$$

This reaction is very advantageous from an environmental point of view because it leads to a radical reduction of NO_2 concentrations in the air. Due to the subsequent oxidation of NO to NO_2

$$2NO + O_2 \rightarrow 2NO_2 \quad (3)$$

followed by Reaction (2), it is possible to further reduce the concentration of NOx in the air.

In some recent studies the formation of the intermediate nitrous acid was observed [9–11], which is even more harmful than the primary reactants NO and NO_2, according to

$$2NO_2 + H_2O \overset{h\nu,TiO_2}{\rightarrow} HONO + HNO_3 \quad (4)$$

$$HONO + h\nu \rightarrow OH + NO \quad (5)$$

However, nitrous acid (HONO) can be subsequently photolyzed to form OH radicals because of its significant absorption cross-section at wavelengths up to 400 nm as is described by Eq. (5) [3]. The photolysis of HONO becomes important as an OH source, especially in the morning. It is believed that the quantum yield for OH production via photolysis is unity at $\lambda < 400$ nm [3]. The extent of reduction of NO_2 to HONO depends on the conditions of the photocatalytic reaction and especially on the performance characteristics of the photocatalyst used. In [12], self-cleaning window glass was used, whose photocatalytic coating was optimized in order to achieve the self-cleaning ability with retaining undiminished transparency and scratch resistance. Consequently, the performance of this glass in the gas-phase photocatalytic reaction was of a secondary importance In [9,10] the photocatalytic coating contained a relatively low concentration of TiO_2 (3–7%) with an overwhelming proportion of the only partially specified binder. The performance of this coating is dominated by the absolutely predominant proportion of the binder. As in the present study a fundamentally different photocatalytic coating was used (see below), the comparison with the published data will help to assess more generally the potential formation of nitrous acid.

Another issue, which should be addressed, is the photolysis of NO_2 and the subsequent gas-phase chemistry and formation of ozone [13]. This possibility was considered in the present study and a long-term photocatalytic test with a very low space velocity (in the range of 0.1 min^{-1}) was carried out, showing that this reaction did not occur in any significant extent.

Although there have been a number of studies of the photocatalytic abatement of NOx under laboratory conditions [2,3,14–17], only very few ones have been conducted under real outdoor conditions. For example, in Antwerp an area of ten thousand square meters was covered with photocatalytic pavement blocks. Even though a reduction in NOx concentrations was observed in both the laboratory and outdoor measurements, it was difficult to draw sound conclusions because the measurement period was too short [18]. Two similar studies were carried out in Italy. In the first, a section of a local street in Bergamo was covered with photocatalytic paving stones, using another, untreated section as a reference. The NOx concentration was monitored for two weeks. Compared to the reference section, a 30–40% reduction in NOx concentration was observed. In the second, the walls of the Umberto I Tunnel in Rome were coated with a photocatalytic cementitious paint and equipped with a UV-lighting system. In this case, a reduction in NOx concentration of over 20% was observed [19]. A French parking lot coated with a photocatalytic paint and illuminated with a UV lamp system was also shown to reduce NOx concentrations [20]. The same authors then tested the efficacy of using TiO_2-mortar panels for photocatalytic degradation of NOx. Three artificial canyon streets were constructed and NOx concentrations were monitored. Depending on the conditions simulated, concentrations decreased in the range of 37–82% [21]. On the other hand, there are also studies published showing that the measured NOx photocatalytic reduction was below the measurement precision errors (1–2%) during the field measurements in an artificial model street canyon in Petosino, Italy [22] or in Leopold II tunnel in Brussels, Belgium [23]. Clearly, the differing conditions of the field experiments carried out, which may be difficult to evaluate completely, played a decisive role.

Considering their various environmental applications, the main advantage of photocatalytic TiO_2-based coatings is that they can be applied to various construction materials used in buildings, pavements, walls and tunnels, among other surfaces. Because of demanding operating conditions, such as highly polluted air, airborne dust, or variations between freezing and hot weather, or rainy and extremely dry periods, the long-term photocatalytic performance and mechanical durability of such photocatalytic coatings are of the utmost importance. Nevertheless, there is a conspicuous lack of data regarding the performance of photocatalytic coatings over longer periods.

In this study, we analyzed the photocatalytic performance of a photocatalytic paint Protectam FN2 produced by the Advanced Materials-JTJ company (Czech Republic). This paint contained a high percentage of Evonik P25 titania material bonded by a highly stable inorganic binder. The pristine Evonik P25 additionally served as an industry standard for the assessment of the photocatalytic performance of the paint. The concentration of NO_2 used in the study equaled 0.1 ppmv, corresponding to 196 $\mu g\, m^{-3}$. This concentration equals the hourly limit according to the EU directive (see above). For NO two concentrations were chosen, namely 1.0 ppmv and 0.1 ppmv. The higher concentration corresponds to the concentration according to the ISO standard, the lower to the concentration according to the above given hourly limit for NO_2. By this choice we reflect the theoretic situation of complete conversion of NO to NO_2.

To obtain reliable data about the effects of weathering, the photocatalytic performance of two-year-old samples taken from a noise barrier located along one of the busiest thoroughfares in Prague was evaluated against that of fresh samples. To obtain as comprehensive set of data as possible, the photocatalytic experiments were carried out at well-defined process conditions in two principally different photocatalytic reactors (laminar-flow and ideally-mixed ones), which provided a much deeper insight into the photocatalytic conversion studied. Further, both coatings were applied to common construction materials, concrete and plaster, which further provides more realistic data. As from the application

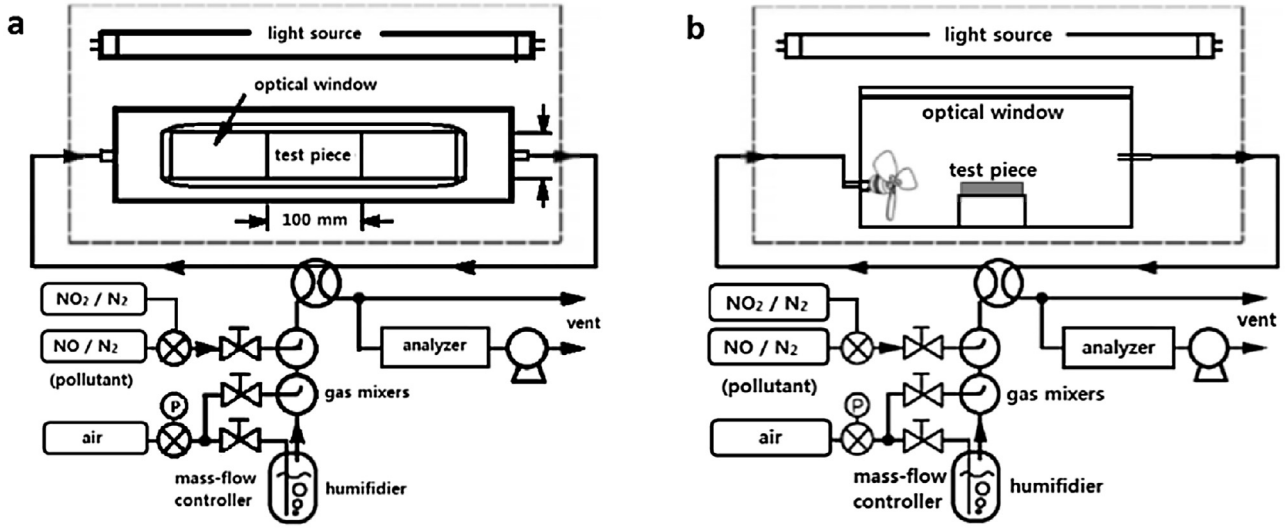

Fig. 1. Experimental set-ups using either the laminar (a) or ideally-mixed (b) flow reactors for the photocatalytic oxidation of gas streams containing low concentrations of nitrogen oxides at the specified humidity [28].

point of view, the long-term stability is of outmost importance. We have shown that the commercial photocatalytic coating Protectam FN2 maintains high efficiency in removing nitrogen oxides from contaminated air even after two years under harsh conditions, owing to the good mechanical properties of the binder used in it.

2. Materials and methods

2.1. Preparation and characterization of photocatalytic coatings

Water suspension of Aeroxide TiO_2 P25 (Evonik, hereinafter referred to as P25) of 74 wt% was applied on plaster and concrete blocks, each 5 × 10 cm in size by spraying using Ryobi P 620 spray gun (Techtronic Industries). The deposition time for each layer was very short of about several seconds. After the application of one layer, there was a technological break for the coating to dry. In this manner, three layers of P25 coating were sprayed creating almost transparent film about 10 μm in thickness with a slightly whitish undertone. Because of the surface roughness of the concrete or plaster supports, the thickness of the coating was determined by an indirect method. First, a comparable layer was deposited on a flat glass. From the mass of the layer, the geometrical area of the glass and the average thickness of the layer as determined by profilometry, its average apparent density was calculated. Using such determined apparent density and the known mass and geometrical size (of approx. 50 cm^2) of the layer deposited on the plaster or concrete, the average thickness was calculated. P25 is a titania photocatalyst that is widely used because of its relatively high level of activity in many photocatalytic reaction systems. It often serves as a standard titania photocatalyst. It contains more than 70% of anatase with a minor amount of rutile (about 20%) and a small percentage of amorphous phase [24]. It exhibits a surface area of about 50 $m^2\ g^{-1}$; the primary particle size is about 21 nm (according to the manufacturer).

The Protectam FN2 coating (produced commercially by Advanced Materials-JTJ, Czech Republic), hereinafter referred to as FN2, is protected by U.S. patent no. 8,647,565 (2009). FN2 consists of about 74% of Aeroxide TiO_2 P25, the remaining part being an inorganic binder. The coating was applied in an analogous way to that of the P25. More data on the properties of the coating is provided in the "Morphological and Structural Properties" section below. The mass of the 50 cm^2 layer of both P25 and FN2 was the same, 0.34 g. Therefore, the samples P25 and FN2 contained 0.34 g and 0.25 g of TiO_2, respectively.

The crystallinity of the coatings was measured using a Siemens D5000 high-resolution X-ray diffractometer operated at 40 kV and 45 mA with Cu Kα radiation (λ = 1.5406 Å). The texture properties of the coatings were determined by analysis of adsorption isotherms of nitrogen at ca 77 K performed with a Micrometrics ASAP 2010 volumetric adsorption unit. The optical properties of the coatings were measured with a Perkin Elmer Lambda 950 UV–vis-NIR spectrometer equipped with Spectralon and gold integration spheres for diffuse reflectance measurements in the UV-NIR region, and with an FT-IR Nicolet 6700 spectrophotometer. The surface morphology of the films was studied with a Joel JSM-6700F scanning electron microscope and a Joel JEM-2100 UHR transmission electron microscope.

2.2. Photocatalytic testing

Testing of photocatalytic activity was performed using two different flow reactor types (Fig. 1), one recommended by ISO 22197-1:2007 and the other by proposed CEN standards. In both reactors, the area of irradiated photocatalytic surface was 50 cm^2 (5 × 10, in cm); the flow rate of air mixture was 3000 $cm^3\ min^{-1}$. The total volume of air treated in 24 h was 4.32 × 10^6 cm^3. The volume of purified air and the area of irradiated photocatalytic surface were the same in both photoreactor. However, the reactors substantially differed in the volume per irradiated area ratio. This ratio was 65 times greater for the ideally-mixed reactor (Table 1).

Ideal mixing in the CEN-standard reactor ensured a uniform composition at any instant of time and any location within the reactor. Uniformity of composition was achieved by intense mixing by a propeller. The volume of the reactor was 5200 cm^3 (18 × 32 × 9, in cm). The space-velocity, which is the number of reactor volumes of feed at specified conditions, which can be treated in the unit time, and the space-time, i.e., the time required to process one reactor volume measured under specified conditions, are given in Table 1.

The ISO 22197-1:2007-standard reactor was characterized by a laminar flow with no mixing or diffusion along the flow path. The free volume of the reactor was 80 cm^3 (5 × 32 × 0.5, in cm), and the linear velocity of the streaming gas was 0.2 $m\ s^{-1}$. The space-velocity and space-time are given in Table 1.

To achieve the required character of flow and degree of mixing, the reactors were systematically optimized. The flow in each test

Table 1
Characteristics of photocatalytic reactors (detail explanation see text).

Type of the flow reactor	Reactor volume (cm^3)	Irradiated area (cm^2)	Volume/irradiated area ($cm^3\ cm^{-2}$)	Air flow ($cm^3\ min^{-1}$)	Space-time[a] (min)	Space-velocity (min^{-1})
Laminar	80	50	1.6	3000	0.027	37.5
Ideally-mixed	5200	50	104	3000	1.7	0.58

[a] another designation "residence time".

reactor was characterized by the residence time distribution, which is the distribution of the time required for the fluid elements (i.e., the stream of air) to pass through the vessel. The residence time distribution of fluid in both types of reactors was determined by the tracer method, using NO in a stream of air. Without UV light irradiation, NO behaved in these experiments as a non-reactive tracer, which did not adsorb on the equipment inner surfaces in a considerable way. In a step experiment at time t = 0, a switch from ordinary fluid (i.e., stream of air only) to fluid with tracer (in this case, 1.0 ppmv of NO in air) was made and the outlet concentration of the tracer was measured over time. In this way, the so-called "F-curves" were determined and used to optimize the performance of both reactor types. If in the optimized mixed reactor the inlet tracer (i.e. NO) concentration rose from zero to one, the corresponded *F*-curve exhibited a characteristic exponential growth in agreement with the theoretic "1−exp (−time/space time)" formula [25]. In the laminar flow reactor, the shape of the *F*-curve was quite different, the inlet step concentration function being transformed to roughly similar outlet step function.

As the gas phase diffusion phenomenon is an important issue to be considered in any reactor engineering experiment, its role in the whole process was carefully analyzed. In the laminar flow reactor, the gas phase diffusion phenomenon can be corrected using a combination of axial dispersion and pure convection models [25–27].

For the ideally-mixed reactor, the situation is relatively simple as owing to the ideal mixing, the gradients within the free volume of the reactor are removed. Consequently, also the effect of the film diffusion resistance or concentration gradients across the gas film surrounding the surface of the solid photocatalyst could not influence the reaction rate, which is typical for the gas-porous catalyst systems [25]. Concerning the pore diffusion resistance, its effect can be expected practically negligible owing to very large width of the pores within the coating (large macropores) compared to the size of gas molecules. The estimation used the correlations between the effectiveness factor and the Thiele modulus showed that the effectiveness factor equaled 1, which corresponds to a negligible pore resistance [25]. For the calculation of the Thiele modulus assessments based on own experiments and the literature data were used [25–27].

Instead of short-term experiments, 3–5 h in duration as given in the mentioned standards, the experiments were prolonged to 24 h, which allowed reaching a steady-state. The stable rate of the photocatalytic reaction in steady-state provides more realistic quantitative results. During the photocatalytic experiments, samples were irradiated by three black-light fluorescent lamps (Philips BLB 15W) in a planar arrangement, emitting a dominant wavelength of 365 nm. The distance between the lamps and the coatings was adjusted to achieve an irradiation intensity of 1.0 mW cm^{-2}. This value corresponds to the sunlight intensity on partly cloudy day in the Middle Europe. On sunny summer days, the intensity is often much larger, up to 4.0 mW cm^{-2}. There was no change in temperature caused by the irradiation arrangements used. Before the photocatalytic experiments, the samples to be tested were cleaned overnight by UV light of a dominant wavelength of 365 nm with irradiation intensity of 2.0 mW cm^{-2} in order to decompose any residual organic matter on them. In the photocatalytic experiment itself, the gas phase containing NO or NO_2 was streamed over the cleansed samples in order to achieve sorption equilibrium between the gas phase and the sample surface, which took about 30 min. The achievement of the sorption equilibrium was determined from the concentration of the nitrogen oxides in the gas stream at the outlet from the photocatalytic reactor. If the concentration of nitrogen oxides was the same at the inlet to the reactor and at the outlet from the reactor, then the sorption equilibrium was achieved. Thus, the removal of nitrogen oxides from the gas phase in the photocatalytic experiment was solely due to photocatalysis, not due to sorption on the surface. The inlet NO concentration was either 1.0 ppmv (corresponding to 1226 $\mu g\ m^{-3}$), or 0.1 ppmv (corresponding to 122.6 $\mu g\ m^{-3}$); the inlet NO_2 concentration was 0.1 ppmv, which corresponds to 188 $\mu g\ m^{-3}$. The reason for the choice of the concentration of 1.0 ppmv of NO was that this same concentration is used in the standards. The concentration of 0.1 ppmv may be encountered in a polluted urban atmosphere due to critical dispersion conditions, on the other hand, it is close to the legal limit for NO_2 concentration in ambient air averaged over one hour (see above).

The studied parameters of the photocatalytic process were as follows:

- inlet pollutant concentration
- character of the flow in the photocatalytic reactor (either laminar or ideally-mixed)
- role of the substrate.

2.3. Photocatalytic efficiency of FN2 samples exposed to the real condition of polluted area in Prague

To obtain realistic data on the effect of aging on the photocatalytic performance of FN2 samples, we performed the comparative photocatalytic measurements of the samples from a test wall located in the proximity of a heavily-trafficked thoroughfare in Prague, used by about 30000 vehicles a day. In this area, the NOx concentration reaches 30–40 $\mu g\ m^{-3}$, and often exceed the permitted NO_2 limit of 40 $\mu g\ m^{-3}$ (0.021 ppmv). The samples of 300 m^2 concrete noise barrier, which had served for two years as a test surface for the FN2 coating, were taken for laboratory testing (Fig. A1).

3. Results and discussion

3.1. Morphological and structural properties of porous coatings

Scanning electron microscopy (SEM) observation showed a significant difference in the surface morphology of the FN2 and P25 coatings. The FN2 coating consisted of a spongy microstructure where the binders (carbonate and sulfate compounds) were covered with TiO_2 particles, which allows direct contact of gas with the TiO_2 surface (Fig. 2b). Fig. 2 shows P25 nanoparticles agglomerated into microscale clusters.

From the comparison of the adsorption isotherms of nitrogen at ca 77 K on the FN2 and P25 coatings it appeared that the former exhibited a larger Brunauer-Emmett-Teller (BET) surface area (82 $m^2\ g^{-1}$) compared to the latter (47 $m^2\ g^{-1}$). Adding the binder clearly led to the creation of a more open texture. From the adsorption isotherms, it further follows that neither mate-

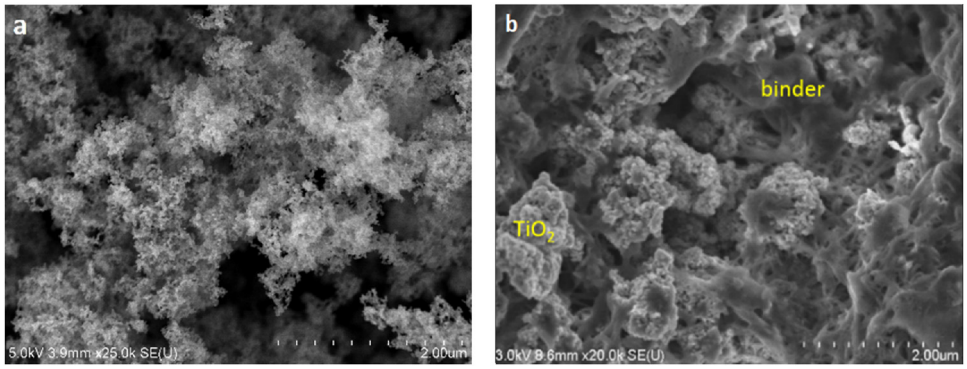

Fig. 2. SEM image of P25 (a) and FN2 (b) dried coatings.

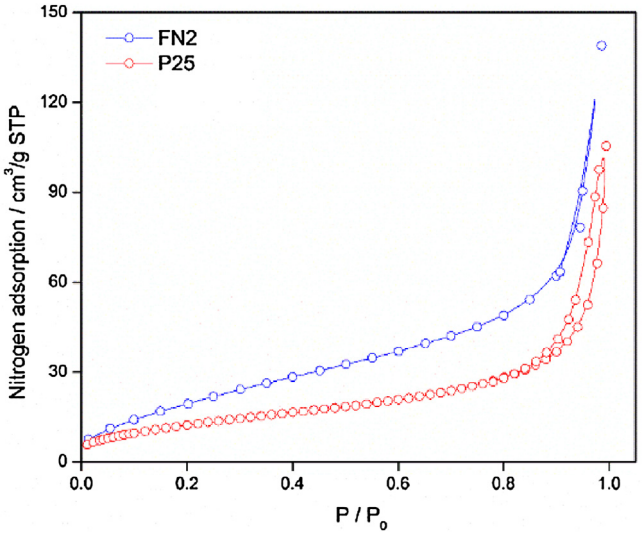

Fig. 3. Nitrogen adsorption isotherms for P25 (red) and FN2 (blue) samples. (For interpretation of the references to colour in this figure legend, the reader is referred to the web version of this article.)

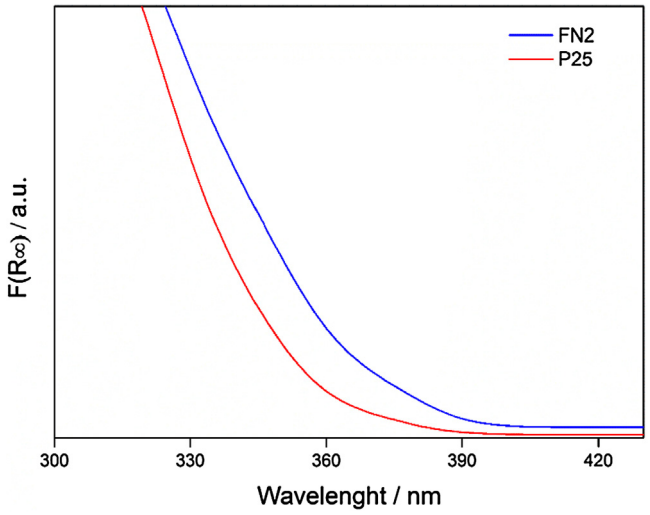

Fig. 4. UV–vis diffuse reflectance spectra of P25 (red) and FN2 (blue) expressed by the Kubelka–Munk function. (For interpretation of the references to colour in this figure legend, the reader is referred to the web version of this article.)

rial contained micropores or mesopores. The width of macropores exceeded 30 nm (Fig. 3).

The diffuse reflectance spectra of the FN2 and P25 coatings showed an absorption edge below 400 nm due to the band gap absorption of the TiO_2 semiconductor (Fig. 4). We plotted the spectra using the Kubelka–Munk *F(R)* function

$$F(R) = \frac{(1-\mathrm{R})}{2R} = \frac{\alpha}{s}, \tag{6}$$

where *R*, α and *s* are the diffuse reflectance, the absorption coefficient and the scattering coefficient, respectively [29,30]. The optical band gap was determined using the following equation

$$(\mathrm{F(R)\,h\nu})^{1/n} \sim \left(\mathrm{h\nu - E_g}\right), \tag{7}$$

where *F(R)*, *h*, ν, E_g and *n* are, respectively, the Kubelka–Munk function, the Planck constant, the oscillation frequency, the band gap and the constant relating to the mode of transition. The minimal-energy state in the conduction band and the maximal-energy state in the valence band are each characterized by a *k*-vector in the Brillouin zone. Two types of band-to-band transitions are suggested. First, direct transitions, where the *k*-vectors are the same and the participation of a phonon is not required to conserve momentum. Second, indirect transitions, where at least one phonon participates in the absorption or emission of a photon to conserve momentum. The constant *n* is 1/2 for the allowed direct transition, 3/2 for the forbidden direct transition or 2 for the allowed indirect transition.

We checked the linearity of the plots against $h\nu$ using $n = 2$ (indirect) or $n = 1/2$ (direct) to assess the mode of transition of a given crystal. More details are provided in the review by Ohtani (2010) [15]. Using the Tauc plot, the optical band gaps E_g for the P25 and FN2 coatings were calculated (Fig. 5) [31]. The absorption data were fitted according to Eq. (5) for both indirect and direct allowed band gap transitions.

Considering the indirect transitions (Fig. 5a), a satisfactory fit was obtained for both samples, giving E_g values of 3.20 and 3.05 eV for P25 and FN2, respectively. For the direct transitions (Fig. 5b), the values of E_g were 3.55 and 3.65 eV, respectively. Checking the approximate range of the straight part of the plot, it was observed to be wider for the indirect transition, which was then selected as more probable.

A significant red shift in the absorbance of FN2 was observed, which could be attributed to the narrowing of the band gap. This effect provides some evidence of interactions between the binders and TiO_2, and also suggests that electron-hole pairs can be generated upon irradiation with longer wavelength light [32]. Consequently, the FN2 coating is expected to show higher activity in the visible region of spectrum than the P25 coating.

Fourier transform infrared spectroscopy provides information of the both coatingsí nature (Fig. 6). We detected Ti–O vibrations for the both samples. The broad peaks at 3400 cm^{-1} and 1650 cm^{-1} corresponds to the surface-adsorbed or chemically bonded water bending vibrations and the hydroxyl (O—H) bending vibrations,

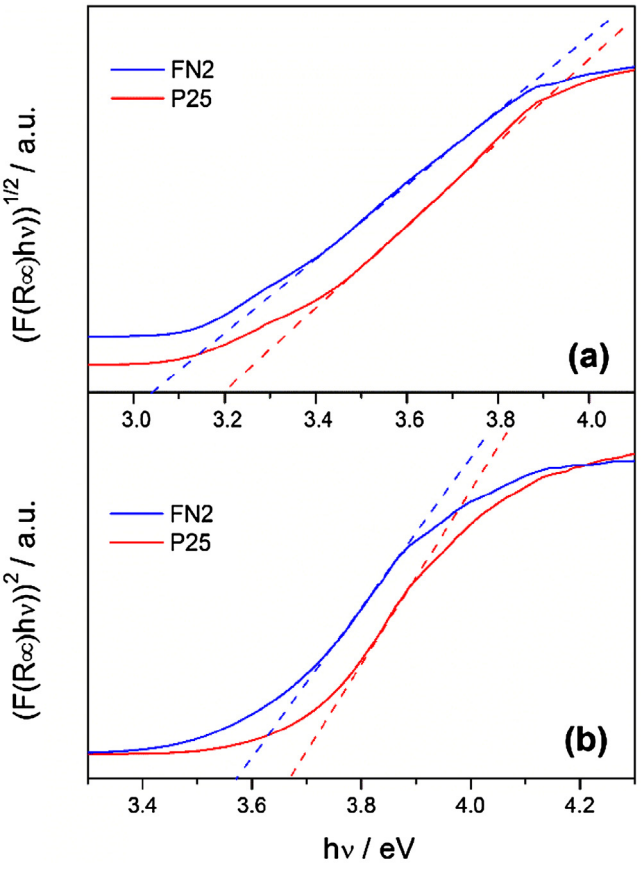

Fig. 5. Determination of the optical band gap (E_g) of P25 (red) and FN2 (blue) coatings using the Tauc plot. (For interpretation of the references to colour in this figure legend, the reader is referred to the web version of this article.)

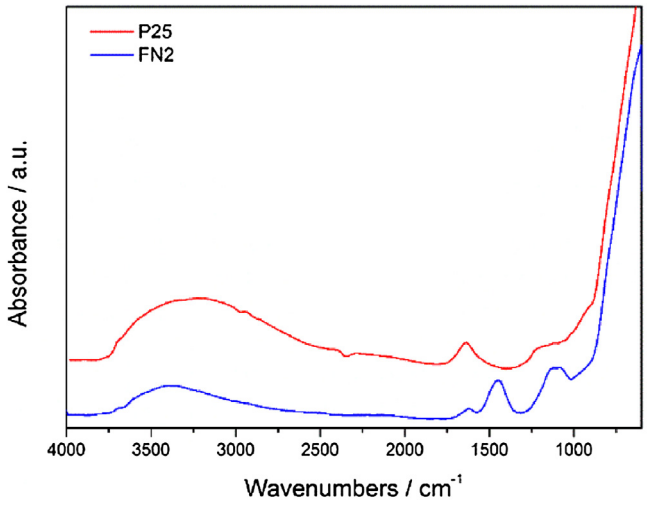

Fig. 6. FT-IR spectra of P25 (red) and FN2 (blue) coatings. (For interpretation of the references to colour in this figure legend, the reader is referred to the web version of this article.)

respectively [33]. According to Yu et al., the hydroxyl groups on the surface of samples contribute to an enhancement of photocatalytic activity [34], because they can interact with photo-generated holes, thereby suppressing the recombination of electron-hole pairs [22,23]. The main peak, centered at about 400–700 cm^{-1} was attributed to Ti—O stretching and Ti—O—Ti bridging stretching modes [35]. Additional vibrations at 1447 cm^{-1}, 1079 cm^{-1} and

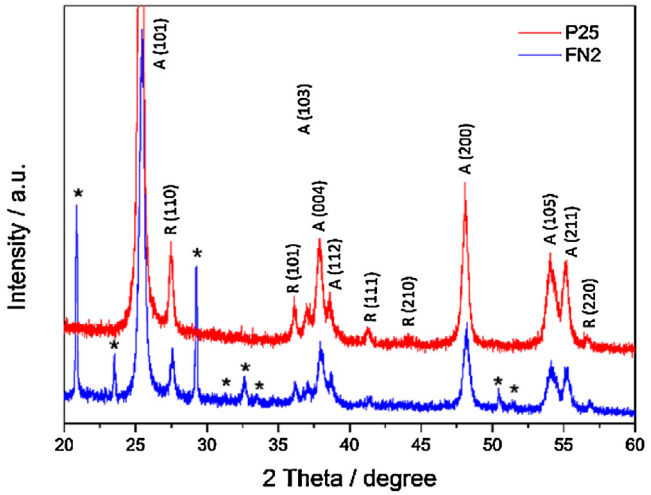

Fig. 7. XRD patterns of P25 (red) and FN2 (blue) coatings. A and R letters denote the anatase and rutile diffraction peaks, respectively. * denote the inorganic binder in FN2 coating. (For interpretation of the references to colour in this figure legend, the reader is referred to the web version of this article.)

1158 cm^{-1} corresponds to the carbonate and sulfate binders in the FN2 coating.

The structural properties of the prepared films were investigated by X-ray diffraction (Fig. 7). The diffraction patterns of both FN2 and P25 exhibited reflections indexed at (101) 25.40°, (103) 37.17°, (004) 37.93°, (112) 38.68°, (200) 47.05°, (105) 54.05°, and (211) 55.18°, corresponding to a tetragonal anatase structure (space group $I4_1/amd$) and indexed at (110) 27.50°, (211) 55.35°, (101) 36.05°, (111) 41.22°, and (210) 44.07° to a tetragonal rutile structure (space group $P4_2/mnm$). The diffractogram of FN2 contained additional diffraction peaks due to the binders (marked by stars), those indexed at 20.87°, 23.53°, 32.64°, 33.50°, and 51.42° belonging to the sulfate binder, and reflections centered at 29.20°, 31.22°, and 50.45° belonging to the carbonate ones.

3.2. Photocatalytic performance of FN2 and P25 coatings

This experimental study generally showed that the concentration of nitrogen oxides can be significantly reduced using photocatalysis on the FN2 and P25 surfaces. The decrease in the NOx concentration was expressed as

a) difference in NOx concentration in the gas stream at the reactor inlet and at the reactor outlet in units ppmv (designated as ΔNOx). This difference was calculated at the beginning of the test and after achieving the steady-state.
b) difference in the NOx concentration in the gas stream at the reactor inlet and at the reactor outlet related to the gas flow rate in units ppmv h m^{-3} (designated as ΔNOx/Q). This difference was calculated after achieving the steady-state.
c) reaction rate of the NOx removal from the gas stream related to a unit irradiated area of the photocatalytic coating in units μmol m^{-2} h^{-1} (designated as r(ΔNOx)), calculated at the beginning of the test and after achieving the steady-state.

The reaction rate of the removal of NOx was chosen for expressing the photocatalytic performance, as it is more suitable than conversion in per cent, which is reactor-bound. Further, the conversion in per cent cannot be used for any calculation of differing situation, e.g. for an estimate of the potential of photocatalysis over an external wall for NOx removal. The reaction rate gives directly how many moles of NOx can be photocatalytically oxidized over

1 m^2 of irradiated photocatalytic surface area in 1 h. Using moles is more suitable than mass units because NO, NOx and HONO have different molar mass. For the ideally-mixed reactor, the reaction rate was calculated from the molar balance at the beginning of the photocatalytic experiment (the initial rate) and after reaching the steady-state. The value at the steady-state is much more meaningful than the initial one, as the reaction rate often decreases fast at the beginning of the experiment. The reason is clearly a deactivation of the most active photocatalytic centers.

Hydrogen peroxide was not detected in the gas phase at the conditions of the experiment by an electroanalytical method [36], i.e., the relative humidity of 50 per cent, temperature of 25 °C and low concentration of nitrogen oxides. If formed hydrogen peroxide is expected to react fast and not to accumulate in the gas phase.

It has been shown that the final product of the photocatalytic oxidation of NO in the presence of TiO_2 is nitric acid (HNO_3), while HONO and NO_2 were identified as intermediate products in the gas phase over the photocatalyst [37–39]. The reaction pathway of photocatalytic oxidation of NO has been discussed in several publications, such as [40,41], most of which propose that the photocatalytic conversion of NO via HONO yields NO_2, which is subsequently oxidized by the attack of water or hydroxyl radicals into the final product, HNO_3. This general conclusion agrees with the observations in the present study that the final product of photocatalytic oxidation captured on the photocatalytic surface of the samples was exclusively HNO_3 (or nitrate), while no nitrites were retained.

Concerning the formation of nitrous acid and nitrites, the analysis of both the photocatalyst surface and the gas phase at the outlet of the reactor was carried out in this study. The analysis of the photocatalyst surface using ion chromatography showed that the final product on the surface was nitric acid and nitrates. The concentration of nitrite as determined by ion chromatography was below the detection limit of less than 0.1 mg L^{-1}.

As nitrous acid is volatile and goes to the gas phase, it was not detected on the surface. The presence of nitrous acid was searched for by the method according to [42]. The data obtained showed that the concentration of nitrous acid was very low, practically at the limit of detection of the method used. The photocatalytic activity related to NO and NO_2 abatement was determined using coatings of P25 and FN2 deposited on plaster and concrete slabs 50 cm^2 in area (Tables 2–4). It was found that the commonly used 3–5 h duration of experiments prescribed in the applicable standards did not provide the required data because of significant changes in the photocatalytic activity occurring after that time. To achieve a steady-state reaction rate, approximately 20 h on stream were found necessary. We focused on the effect of several important processing parameters on the photocatalytic activity of the samples studied. An analysis of those effects is provided in the following paragraphs. Typical examples of variations in the reaction rate depending on the time allowed for the inlet streams containing either NO or NO_2 are shown in Figs. 8 and 9.

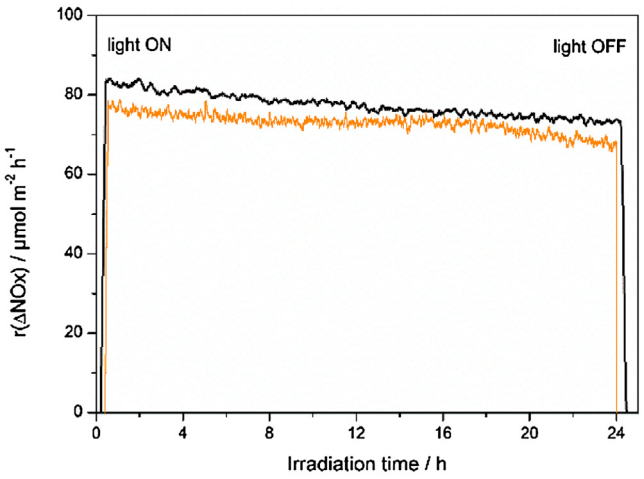

Fig. 8. Rate of photocatalytic reaction of FN2 coated on concrete in both reactors at the inlet NO concentration of 0.1 ppmv and relative humidity (RH) of 50%. Laminar flow reactor (black), ideally-mixed flow reactor (orange). (For interpretation of the references to colour in this figure legend, the reader is referred to the web version of this article.)

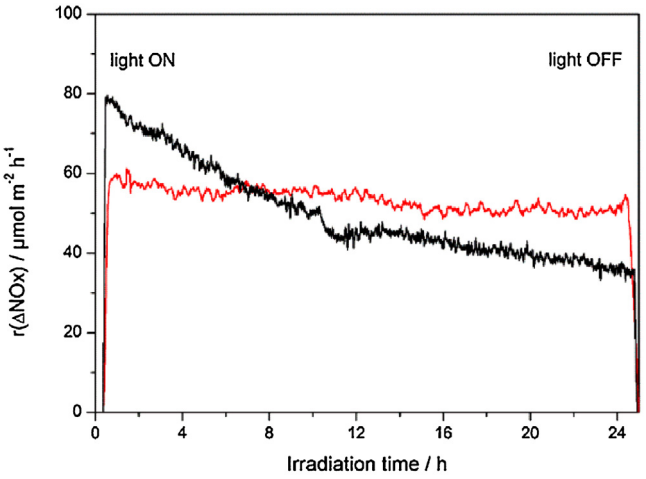

Fig. 9. Rate of photocatalytic reaction of FN2 coated on plaster in ideally-mixed flow reactor (red) and on concrete in laminar flow reactor (black), both at the inlet NO_2 concentration of 0.1 ppmv and relative humidity (RH) of 50%. (For interpretation of the references to colour in this figure legend, the reader is referred to the web version of this article.)

3.2.1. Ratio of the initial and steady-state reaction rate of the removal of NOx from the gas stream, inlet NO concentration of 0.1 and 1.0 ppmv

Generally, the data showed that the initial reaction rate was greater than the steady-state one. However, there was a substantial effect observed with regard to the substrate (Table 2). If concrete was used as support, the decrease in the reaction rate was rather small, no more than 20 per cent. This small decrease was observed for both P25 and FN2, as well as for both of the inlet NO concentrations used. If plaster was the substrate, the decrease was much greater, often more than 50 per cent. This important influence of the character of the substrate may be connected to the substrates' mechanical (strength, durability and stability), structure (chemical composition) or texture (porosity, surface area) properties. Interestingly, the initial reaction rate at the inlet NO concentration of 1.0 ppmv was as much as four times higher if plaster was used as the substrate. However, this high initial reaction rate was followed by rather steep decrease, which did not occur when concrete was the substrate.

3.2.2. FN2 vs. P25

Comparison of the photocatalytic performance of P25 (100% titanium dioxide) and FN2 (74% of P25 with 26% of binder) provided an interesting outcome (Fig. 10). The reaction rate with the FN2 coating was higher than that recorded with P25, even though the percentage of titania in the FN2 coating was lower. For instance, the reaction rate with FN2 coating on concrete in the both laminar and ideally-mixed flow reactors at the inlet NO concentration of 1.0 ppmv was 40 and 49 per cent higher, respectively, than the corresponding reaction rate of P25. A possible reason might be a

Table 2
Decrease in the NOx concentration due to photocatalytic oxidation on FN2 and P25 coatings for the inlet NO concentrations of 1.0 and 0.1 ppmv at relative humidity (RH) of 50%.

Coating	Reactor	Substrate	$[NO]_{in}$ (ppmv)	Initial ΔNOx (ppmv)	Steady-state ΔNOx (ppmv)	Steady-state ΔNOx/Q (ppmv h m^{-3})	Initial r(ΔNOx) (μmol m^{-2} h^{-1})	Steady-state r(ΔNOx) (μmol m^{-2} h^{-1})
FN2	LFR	concrete	1.0	0.120	0.120	0.67	176	176
		plaster	1.0	0.500	0.240	1.33	735	353
		concrete	0.1	0.057	0.050	0.28	84	74
		plaster	0.1	0.034	0.017	0.09	50	25
	CSTR	concrete	1.0	0.470	0.420	2.33	691	617
		plaster	1.0	0.720	0.350	1.94	1058	514
		concrete	0.1	0.054	0.045	0.25	79	66
		plaster	0.1	0.042	0.032	0.18	63	47
P25	LFR	concrete	1.0	0.100	0.080	0.44	147	118
		plaster	1.0	0.430	0.160	0.89	632	235
	CSTR	concrete	1.0	0.380	0.300	1.67	559	441
		plaster	1.0	0.600	0.280	1.56	882	412

LFR, laminar flow reactor; CSTR, ideally-mixed flow reactor; $[NO]_{in}$, inlet concentration of NO; ΔNOx, initial and steady-state decrease in the concentration of NOx in the gas stream; ΔNOx/Q, steady-state decrease in the NOx concentration related to a unit volume of the streaming gas; r(ΔNOx), corresponding reaction rate of the removal of NOx from the gas stream. Steady-state data determined after 24 h on stream.

Table 3
Decrease in the NOx concentration due to the photocatalytic oxidation on FN2 and P25 coatings for the inlet NO_2 concentration of 0.1 ppmv at relative humidity (RH) of 50%.

Coating	Reactor	Substrate	$[NO_2]_{in}$ (ppmv)	Initial ΔNOx (ppmv)	Steady-state ΔNOx (ppmv)	Steady-state ΔNOx/Q (ppmv h m^{-3})	Initial r(ΔNOx) (μmol m^{-2} h^{-1})	Steady-state r(ΔNOx) (μmol m^{-2} h^{-1})
FN2	LFR	concrete	0.1	0.054	0.024	0.13	79	35
		plaster	0.1	0.036	0.036	0.20	53	53
	CSTR	concrete	0.1	0.037	0.022	0.12	54	32
		plaster	0.1	0.040	0.040	0.22	59	59
P25	LFR	concrete	0.1	0.042	0.015	0.08	61	22
		plaster	0.1	0.028	0.025	0.14	41	37
	CSTR	concrete	0.1	0.024	0.015	0.08	35	22
		plaster	0.1	0.029	0.026	0.14	42	38

LFR, laminar flow reactor; CSTR, ideally-mixed flow reactor; $[NO_2]_{in}$, inlet concentration of NO_2; ΔNOx, initial and steady-state decrease in the concentration of NOx in the gas stream; ΔNOx/Q, steady-state decrease in the NOx concentration related to a unit volume of the streaming gas; r(ΔNOx), corresponding reaction rate of the removal of NOx from the gas stream. Steady-state data determined after 24 h on stream.

Table 4
Comparison of the photocatalytic activity of a fresh FN2 coating with that of a two-year-old one applied to concrete and tested in the laminar flow reactor (LFR) at relative humidity (RH) of 50%. The inlet concentration of NO was either 1.0 or 0.1 ppmv, that of NO_2 0.1 ppmv.

Sample	Substrate	Gas	$[NOx]_{in}$ (ppmv)	Initial ΔNOx (ppmv)	Steady-state ΔNOx (ppmv)	Steady-state ΔNOx/Q (ppmv h m^{-3})	Initial r(ΔNOx) (μmol m^{-2} h^{-1})	Steady-state r(ΔNOx) (μmol m^{-2} h^{-1})
fresh	concrete	NO	1.0	0.120	0.120	0.67	176	147
aged		NO	1.0	0.180	0.050	0.28	220	74
fresh	concrete	NO	0.1	0.057	0.050	0.28	84	74
aged		NO	0.1	0.048	0.040	0.22	71	59
fresh	concrete	NO_2	0.1	0.040	0.040	0.22	59	59
aged		NO_2	0.1	0.037	0.018	0.10	55	27

$[NOx]_{in}$, inlet concentration of NO or NO_2; ΔNOx, initial and steady-state decrease in the concentration of NOx in the gas stream; ΔNOx/Q, steady-state decrease in the NOx concentration related to a unit volume of the streaming gas; r(ΔNOx), corresponding reaction rate of the removal of NOx from the gas stream. Steady-state data determined after 24 h on stream.

beneficial effect of larger surface area of FN2 (82 m^2 g^{-1}) compared to P25 (47 m^2 g^{-1}).

3.2.3. *Effect of concentration and velocity gradients on the reaction rate*

The experiments in the laminar flow reactor (with radial concentration and velocity gradients) and in the gradientless ideally-mixed flow reactor showed that the character of flow and the degree of mixing within the reactor played a decisive role in the reaction. At the inlet NO concentration of 1.0 ppmv, the reaction rate in the ideally-mixed reactor was higher than that in the laminar flow one. Typically, the reaction rate for FN2 and P25 (both on concrete) was about 3.5 times higher in the ideally-mixed reactor than in the laminar flow reactor. Clearly, the limited transfer of matter (i.e., NO and O_2 molecules) and momentum in the radial direction was a determining factor in the reaction rate that slowed down the process of NO conversion. In the gradientless ideally-mixed reactor, no such detrimental effect was operative. At the lower inlet NO concentration of 0.1 ppmv, the substantially slower reaction itself started becoming the rate-determining step and the effect of concentration and velocity gradients was partly suppressed.

3.2.4. *Effect of the inlet NO concentration on the reaction rate*

The inlet concentration of NO had a substantial influence on the reaction rate in the both reactors (Table 2). A comparison of the data obtained for the FN2 coating in the laminar flow reactor

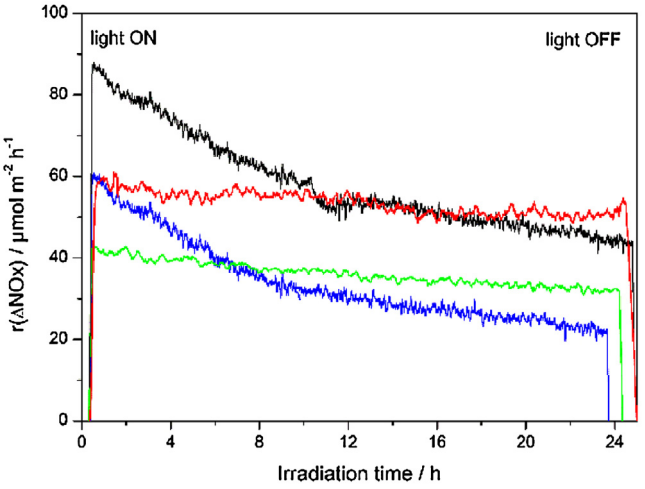

Fig. 10. Comparison of the photocatalytic reaction rates of FN2 and P25 in the both ideally-mixed and laminar flow reactors at the inlet NO_2 concentration of 0.1 ppmv and relative humidity (RH) of 50%. FN2 (black) and P25 (blue) coated on concrete in laminar flow reactor; FN2 (red) and P25 (green) coated on plaster in ideally-mixed flow reactor. (For interpretation of the references to colour in this figure legend, the reader is referred to the web version of this article.)

showed that the reaction rate was roughly proportional to the inlet NO concentration, i.e. at the inlet NO concentration of 1.0 ppmv, it was roughly ten times higher than for the inlet concentration of 0.1 ppmv. This relationship indicates that enhanced deposition of nitric acid due to higher inlet NO concentrations and higher reaction rate did not affect the result.

3.2.5. Experiments with NO_2

The results obtained for the photocatalytic oxidation of NO_2 were very interesting (Table 3), because such data is very rarely encountered in the literature. The NO_2 concentration used in the study equals 0.1 ppmv, which corresponds to the limit of the European directive on NO_2 concentration in ambient air averaged over 1 h. The trends differed from those for NO. First, the difference in the reaction rate at the initial of reaction and in the steady-state was much smaller for the both P25 and FN2 coatings applied on plaster than on concrete. On plaster, the reaction rate practically did not change, but on concrete the decrease was between 40 and 60 per cent. Additionally, the steady-state reaction rate on the coatings applied on plaster was consistently 1.5–1.8 times higher in comparison with the coatings on concrete. The reason for this might be connected with the different physico-chemical properties of the two nitrogen oxides. However, the true explanation of this observation has not been ascertained yet and will be addressed in our follow-up research. Finally, we observed that reverse reduction of NO_2 to NO was negligible.

3.2.6. Comparison of the laminar and ideally-mixed flow reactors

Reaction rates for the inlet NO and NO_2 concentrations of 0.1 ppmv on the FN2 coating were mostly comparable for the both reactors. In these reactors, the same volume per time of air was purified, however, the ratio of the reactor volume and the area of irradiated photocatalytic coating were substantially different. For laminar and ideally-mixed reactor this ratio equaled 1.6 and 104 $cm^3\ cm^{-2}$, i.e. it was 65 times greater for the latter reactor. The much greater volume to irradiated area ratio for the ideally-mixed reactor was clearly compensated by equally longer space-time (residence time).

3.3. Photocatalytic performance of the FN2 coating in the real conditions: environmental impact

The laboratory results showed that even two years after its application on the surface of noise barriers along a busy thoroughfare in Prague, FN2 photocatalytic coating maintained high effectivity (Table 4). For the inlet NO concentration of 0.1 ppmv (122.6 $\mu g\ m^{-3}$), corresponding to highly polluted air, the decrease in the reaction rate was only 20 per cent. For the same concentration of inlet NO_2, the decrease was larger, 50 per cent, which agrees with the observations reported in the preceding paragraphs.

The adhesion of the photocatalytic material to the substrate is crucial to preventing deterioration and loss of photocatalytic activity. In comparison with P25, the FN2 coating has substantial advantages, especially its stable binder, which ensures very good cohesion of the layer and its strong adhesion to the construction material underneath. Without any binder (P25), nanoparticles tend to stick to the surface electrostatically, which is not sufficient to achieve satisfactory strength and durability. The choice of a suitable binder for outdoor application is decisive, as washout of particles should be avoided. At the same time, care has to be taken that the binder does not coat the photocatalyst particles completely, thus preventing their activity. In the case of FN2, which contains inorganic binders, the adhesion to the underlying surface of 3 MPa (as determined by ISO EN 1504-2: 2004) is very good as evidenced by durability tests. Mechanical testing showed that in the FN2 composite coating, all the nanoparticles were interconnected and firmly anchored in a porous structure. Consequently, the release of individual nanoparticles from the composite was virtually impossible, which is important not only from a technological point of view, but also with regard to potential adverse effects on the environment and health (see the Appendix A for details).

4. Conclusions

To sum up, this study has shown that the concentration of both NO and NO_2 in the air can be significantly reduced by the photocatalytic process. However, the efficiency of that process depends on a number of parameters, which for the most part have not been addressed in prior studies, such as the character of air flow and the degree of mixing, the effect of the inlet concentration (not only of NO but also of NO_2), and the use of realistic materials as substrates for the photocatalytic coating (such as concrete and plaster).

Another important issue is the durability of the performance of photocatalytic coatings under real-world conditions. We have shown that the commercial photocatalytic coating Protectam FN2 maintains high efficiency in removing nitrogen oxides from contaminated air even after two years under harsh conditions, owing to the good mechanical properties of the binder used in it.

The transfer of experimental data from the laboratory to "on-site efficiency" is not easy because of the large number of parameters that must be taken into account. The present study, which has addressed several potentially important parameters, has attempted to provide some clue. As the next step in our systematic research, we have started an extensive study aimed at more reliable prediction of the performance of photocatalytic coatings under real conditions, using more advanced engineering models.

Acknowledgments

The authors are grateful to the Czech Science Foundation (GACR) for financial support (Grant No. 17-18972S). The authors also thank Research Infrastructure NanoEnviCz, supported by the Ministry of Education Youth and Sports of the Czech Republic (Project No. LM2015073), for providing access to UV–vis and FT-IR spectropho-

tometers. The authors further thank the Technical and Test Institute for Construction (Prague, Czech Republic) for carrying out the mechanical testing of the FN2 coating. Finally, they thank B. Sánchez (Universidad Complutense de Madrid, Madrid, Spain) for carrying out the ion-chromatographic analysis for determination of nitrates and nitrites in the reaction deposits on the surface of the photocatalytic coatings.

Appendix A. Testing the mechanical properties of FN2 coating

In accordance with a certified test (standard EN 1504-2: 2004), the adhesion of FN2 to the surface was 3 MPa. To carry out the mechanical tests, double-sided adhesive tape was first pressed on the wall coated with FN2 at several points. After that, fragments adhering to the tape were removed from the wall using a pull-off strength of 0.45 MPa. From analysis by scanning electron microscopy images, it appeared that the majority of the captured fragments of FN2 were from 15 to 100 μm in size, and only a negligible fraction of them was smaller than 10 μm (Fig. A2). Detailed analysis of the breakaway layer of FN2 further showed that the area of breakage was homogenous. It follows that the large, compact pieces broken off the composite coating were formed from much smaller (about 1000 times) particles, while the individual nanoparticles were tightly embedded within the composite nanostructure.

Fig. A1. Taking samples from a noise barrier treated with FN2 two years earlier, on a sunny day without rain for at least 7 days before.

References

[1] Cristina Guerreiro, Frank de Leeuw, Valentin Foltescu, Alberto González Ortiz, Air Quality in Europe — 2015 Report, 2015, http://dx.doi.org/10.2800/62459.
[2] Y. Boyjoo, H. Sun, J. Liu, V.K. Pareek, S. Wang, A review on photocatalysis for air treatment: from catalyst development to reactor design, Chem. Eng. J. 310 (2017) 537–559, http://dx.doi.org/10.1016/j.cej.2016.06.090.
[3] Y. Sadanaga, J. Matsumoto, Y. Kajii, Photochemical reactions in the urban air: recent understandings of radical chemistry, J. Photochem. Photobiol. C Photochem. Rev. 4 (2003) 85–104, http://dx.doi.org/10.1016/S1389-5567(03)00006-6.
[4] C. Kessler, U. Platt, Nitrous acid in polluted air masses – Sources and formation pathways, in: Physico-Chemical Behav. Atmos. Pollut., D. Reidel Dordrecht, 1984, pp. 412–422.
[5] J.N. Pitts, H.W. Biermann, A.M. Winer, Spectroscopic identification and measurement of gaseous nitrous-acid in dilute auto exhaust, Atmos. Environ. 18 (1984) 847–854.
[6] T.W. Kirchstetter, R.A. Harley, D. Littlejohn, Measurement of nitrous acid in motor vehicle exhaust, Environ. Sci. Technol. 30 (1996) 2843–2849, http://dx.doi.org/10.1021/es960135y.
[7] R. Kurtenbach, K.H. Becker, J.A.G. Gomes, J. Kleffmann, J.C. Lörzer, M. Spittler, P. Wiesen, R. Ackermann, A. Geyer, U. Platt, Investigations of emissions and heterogeneous formation of HONO in a road traffic tunnel, Atmos. Environ. 35 (2001) 3385–3394, http://dx.doi.org/10.1016/S1352-2310(01)00138-8.
[8] N. Negishi, K. Takeuchi, Preparation of TiO_2 thin film photocatalysts by dip coating using a highly viscous solvent, J. Sol-Gel Sci. Technol. 22 (2001) 23–31, http://dx.doi.org/10.1023/A:1011204001482.
[9] A. Gandolfo, L. Rouyer, H. Wortham, S. Gligorovski, The influence of wall temperature on NO_2 removal and HONO levels released by indoor photocatalytic paints, Appl. Catal. B Environ. 209 (2017) 429–436, http://dx.doi.org/10.1016/j.apcatb.2017.03.021.
[10] A. Gandolfo, V. Bartolomei, E. Gomez Alvarez, S. Tlili, S. Gligorovski, J. Kleffmann, H. Wortham, The effectiveness of indoor photocatalytic paints on NOx and HONO levels, Appl. Catal. B Environ. 166–167 (2015) 84–90, http://dx.doi.org/10.1016/j.apcatb.2014.11.011.
[11] M.E. Monge, B. D'Anna, C. George, Nitrogen dioxide removal and nitrous acid formation on titanium oxide surfaces—an air quality remediation process? Phys. Chem. Chem. Phys. 12 (2010) 8991, http://dx.doi.org/10.1039/b925785c.
[12] J.M. Langridge, R.J. Gustafsson, P.T. Griffiths, R.A. Cox, R.M. Lambert, R.L. Jones, Solar driven nitrous acid formation on building material surfaces containing titanium dioxide: a concern for air quality in urban areas? Atmos. Environ. 43 (2009) 5128–5131, http://dx.doi.org/10.1016/j.atmosenv.2009.06.046.
[13] M.E. Monge, C. George, B. D'Anna, J.F. Doussin, A. Jammoul, J. Wang, G. Eyglunent, G. Solignac, V. Daële, A. Mellouki, Ozone formation from illuminated titanium dioxide surfaces, J. Am. Chem. Soc. 132 (2010) 8234–8235, http://dx.doi.org/10.1021/ja1018755.
[14] J. Lasek, Y. Yu, J.C.S. Wu, Removal of NOx by photocatalytic processes, J. Photochem. Photobiol. C Photochem. Rev. 14 (2013) 29–52, http://dx.doi.org/10.1016/j.jphotochemrev.2012.08.002.

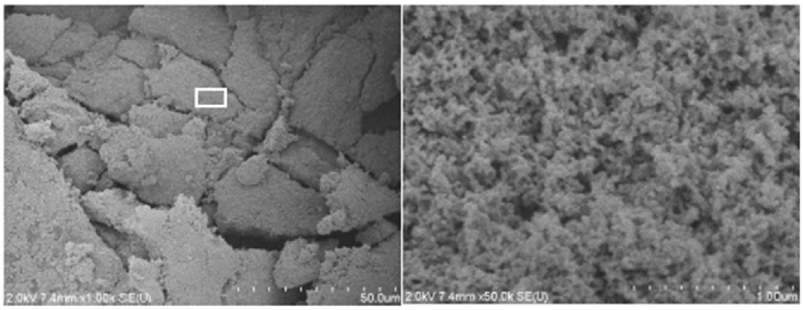

Fig. A2. SEM image of detached fragments.

[15] B. Ohtani, Photocatalysis A to Z-what we know and what we do not know in a scientific sense, J. Photochem. Photobiol. C Photochem. Rev. 11 (2010) 157–178, http://dx.doi.org/10.1016/j.jphotochemrev.2011.02.001.
[16] S.W. Verbruggen, TiO_2 photocatalysis for the degradation of pollutants in gas phase: from morphological design to plasmonic enhancement, J. Photochem. Photobiol. C Photochem. Rev. 24 (2015) 64–82, http://dx.doi.org/10.1016/j.jphotochemrev.2015.07.001.
[17] S. Ifang, M. Gallus, S. Liedtke, R. Kurtenbach, P. Wiesen, J. Kleffmann, Standardization methods for testing photo-catalytic air remediation materials: problems and solution, Atmos. Environ. 91 (2014) 154–161, http://dx.doi.org/10.1016/j.atmosenv.2014.04.001.
[18] E. Boonen, A. Beeldens, Recent photocatalytic applications for air purification in Belgium, Coatings 4 (2005) 553–573, http://dx.doi.org/10.3390/coatings4030553.
[19] G.L. Guerrini, Photocatalytic performances in a city tunnel in Rome: NOx monitoring results, Constr. Build. Mater. 27 (2012) 165–175, http://dx.doi.org/10.1016/j.conbuildmat.2011.07.065.
[20] T. Maggos, J.G. Bartzis, M. Liakou, C. Gobin, Photocatalytic degradation of NOx gases using TiO_2-containing paint: a real scale study, J. Hazard. Mater. 146 (2007) 668–673, http://dx.doi.org/10.1016/j.jhazmat.2007.04.079.
[21] T. Maggos, A. Plassais, J.G. Bartzis, Photocatalytic degradation of NOx in a pilot street canyon configuration using TiO_2 −mortar panels, Environ. Monit. Assess. (2008) 35–44, http://dx.doi.org/10.1007/s10661-007-9722-2.
[22] M. Gallus, R. Ciuraru, F. Mothes, V. Akylas, F. Barmpas, A. Beeldens, F. Bernard, E. Boonen, A. Boreaave, M. Cazaunau, N. Charbonnel, H. Chen, V. Daele, Y. Dupart, C. Gaimoz, B. Grosselin, H. Herrmann, S. Ifang, R. Kurtenbach, M. Maille, I. Marjanovic, V. Michoud, A. Mellouki, K. Miet, N. Moussiopoulos, L. Poulain, P. Zapf, C. George, J.F. Doussin, J. Kleffmann, Photocatalytic abatement results from a model street canyon, Environ. Sci. Pollut. Res. 22 (2015) 18185–18196, http://dx.doi.org/10.1007/s11356-015-4926-4.
[23] M. Gallus, V. Akylas, F. Barmpas, A. Beeldens, E. Boonen, A. Boreave, M. Cazaunau, H. Chen, V. Daele, J.F. Doussin, Y. Dupart, C. Gaimoz, C. George, B. Grosselin, H. Herrmann, S. Ifang, R. Kurtenbach, M. Maille, A. Mellouki, K. Miet, F. Mothes, N. Moussiopoulos, L. Poulain, R. Rabe, P. Zapf, J. Kleffmann, Photocatalytic de-pollution in the Leopold II tunnel in Brussels: NOx abatement results, Build. Environ. 84 (2015) 125–133, http://dx.doi.org/10.1016/j.buildenv.2014.10.032.
[24] B. Ohtani, D. Li, R. Abe, What is Degussa (Evonik) P25? Crystalline composition analysis, reconstruction from isolated pure particles and photocatalytic activity test, J. Photochem. Photobiol. A: Chem. 216 (2010) 179–182, http://dx.doi.org/10.1016/j.jphotochem.2010.07.024.
[25] O. Levenspiel, Chemical Reaction Engineering, 3rd edition, John Wiley & Sons, 1999.
[26] T.K. Sherwood, R.C. Reid, J.M. Prausnitz, The Properties of Gases and Liquids, 3rd edition, 1977.
[27] E.N. Lightfoot, R.B. Bird, W.E. Stewart, Transport Phenomena, John Wiley & Sons, 1965.
[28] J. Rathousky, V. Kalousek, V. Yarovyi, M. Wark, J. Jirkovsky, A low-cost procedure for the preparation of mesoporous layers of TiO 2 efficient in the environmental clean-up, J. Photochem. Photobiol. A: Chem. 216 (2010) 126–132, http://dx.doi.org/10.1016/j.jphotochem.2010.06.002.
[29] P. Kubelka, New contributions to the optics of intensely light-scattering materials. Part I, J. Opt. Soc. Am. 38 (1948) 448–457, http://dx.doi.org/10.1364/JOSA.38.000448.
[30] V. Džimbeg-malčić, Ž. Barbarić-mikočević, K. Itrić, Kubelka-Munk theory in describing optical properties of paper (1), Tech. Gaz. 18 (2011) 117–124, http://dx.doi.org/10.1017/CBO9781107415324.004.
[31] A. Tauc, J. Grigorovici, R. Vancu, Optical properties and electronic structure of amorphous germanium, Mater. Res. Bull. 3 (1966) 37–46, http://dx.doi.org/10.1016/0025-5408(68)90023-8.
[32] S. Kalathil, M.M. Khan, S.A. Ansari, J. Lee, M.H. Cho, Band gap narrowing of titanium dioxide (TiO_2) nanocrystals by electrochemically active biofilms and their visible light activity, Nanoscale 5 (2013) 6323–6326, http://dx.doi.org/10.1039/c3nr01280h.
[33] C. Arrouvel, M. Digne, M. Breysse, H. Toulhoat, P. Raybaud, Effects of morphology on surface hydroxyl concentration: a DFT comparison of anatase-TiO_2 and γ-alumina catalytic supports, J. Catal. 222 (2004) 152–166, http://dx.doi.org/10.1016/j.jcat.2003.10.016.
[34] J. Yu, G. Wang, B. Cheng, M. Zhou, Effects of hydrothermal temperature and time on the photocatalytic activity and microstructures of bimodal mesoporous TiO_2 powders, Appl. Catal. B Environ. 69 (2007) 171–180, http://dx.doi.org/10.1016/j.apcatb.2006.06.022.
[35] J. Yu, H. Yu, Facile synthesis and characterization of novel nanocomposites of titanate nanotubes and rutile nanocrystals, Mater. Chem. Phys. 100 (2006) 507–512, http://dx.doi.org/10.1016/j.matchemphys.2006.02.002.
[36] M.A. Komkova, E.E. Karyakina, F. Marken, A.A. Karyakin, Hydrogen peroxide detection in wet air with a prussian blue based solid salt bridged three electrode system, Anal. Chem. 85 (2013) 2574–2577, http://dx.doi.org/10.1021/ac303761h.
[37] R. Dillert, J. Stötzner, A. Engel, D.W. Bahnemann, Influence of inlet concentration and light intensity on the photocatalytic oxidation of nitrogen(II) oxide at the surface of Aeroxide TiO_2 P25, J. Hazard. Mater. 211–212 (2012) 240–246, http://dx.doi.org/10.1016/j.jhazmat.2011.11.041.
[38] J. Chen, C. sun Poon, Photocatalytic construction and building materials: from fundamentals to applications, Build. Environ. 44 (2009) 1899–1906, http://dx.doi.org/10.1016/j.buildenv.2009.01.002.
[39] S. Laufs, G. Burgeth, W. Duttlinger, R. Kurtenbach, M. Maban, C. Thomas, P. Wiesen, J. Kleffmann, Conversion of nitrogen oxides on commercial photocatalytic dispersion paints, Atmos. Environ. 44 (2010) 2341–2349, http://dx.doi.org/10.1016/j.atmosenv.2010.03.038.
[40] M.M. Ballari, Q.L. Yu, H.J.H. Brouwers, Experimental study of the NO and NO_2 degradation by photocatalytically active concrete, Catal. Today 161 (2011) 175–180, http://dx.doi.org/10.1016/j.cattod.2010.09.028.
[41] S. Devahasdin, C. Fan, K. Li, D.H. Chen, TiO_2 photocatalytic oxidation of nitric oxide: transient behavior and reaction kinetics, J. Photochem. Photobiol. A Chem. 156 (2003) 161–170, http://dx.doi.org/10.1016/S1010-6030(03)00005-4.
[42] J. Kleffmann, P. Wiesen, Technical note: quantification of interferences of wet chemical HONO LOPAP measurements under simulated polar conditions, Atmos. Chem. Phys. 8 (2008) 6813–6822, http://dx.doi.org/10.5194/acp-8-6813-2008.